INTERNATIONAL JOURNAL FOR NUMERICAL METHODS IN FLUIDS, VOL. 2, 277–297 (1982)

HERMITIAN SPACE–TIME FINITE ELEMENTS FOR ESTUARINE MASS TRANSPORT

R. J. SOBEY

Department of Civil and Systems Engineering, James Cook University, Townsville 4811, Australia

SUMMARY

Space–time finite element solutions of the convection–dispersion equation using higher-order nodal continuity and Hermitian polynomial shape functions are described. Five separate elements ranging from a complete linear element with $C^{0,0}$ nodal continuity to a complete first-order Hermitian element with $C^{1,1}$ nodal continuity are subjected to detailed analysis. Wave deformation analyses identify the source of leading or trailing edge oscillations, trailing edge oscillations being the major source of difficulty. These observations are confirmed by numerical experiments which further demonstrate the potential of higher-order nodal continuity. The performance of the complete first-order Hermitian element is quite satisfactory and measurably superior to the linear element.

KEY WORDS Advection Convection Estuary Finite Element Hermite Polynomials Diffusion Dispersion Transport

INTRODUCTION

Estuarine mass transport is described by a generalized form of the classical unsteady convection–dispersion equation and any numerical solution algorithm that maintains an Eulerian framework has potential problems with numerical dispersion and solution oscillations. It is generally recognized that the numerical difficulties originate with the convective term and are particularly severe where there is poor spatial resolution, although there is little general agreement regarding the most satisfactory solution algorithm. Numerous algorithms have been proposed in the literature and all three appropriate numerical solution techniques—the method of characteristics, the finite difference method and the finite element method—have been used in a wide variety of forms. This paper describes one such alternative, using space–time finite elements and higher-order Hermitian shape functions. This approach has received relatively little attention but appears to have some potential in the estuarine environment. Five variations on this approach are investigated, in the context of wave deformation analyses and numerical experiments, and the overall results give a good perspective to the potential of higher-order numerical algorithms for the convection–dispersion equation.

This study was initiated in the context of mass transport in a narrow but well-mixed estuarine channel. Estuarine conditions provide a severe test of any solution algorithm. Flows may vary from nothing to large values in both directions and concentration gradients may vary in a similar manner. A successful solution algorithm must accommodate this range of operational conditions. In dimensionless terms with the space step Δx and the time step Δt as the characteristic length and time scales, the numerical solution is dependent on the flow

0271–2091/82/030277–21$02.10

Received 7 October 1981
Revised 15 December 1981

parameter $U\,\Delta t/\Delta x$ and the dispersion parameter $E\,\Delta t/\Delta x^2$, where $U(x, t)$ is the cross-sectionally averaged flow velocity including tidal and fresh water components and E the longitudinal dispersion coefficient. In a typical estuarine situation the flow parameter might range in magnitude up to about three and the dispersion parameter would be small and of order 0·1. That the flow parameter frequently exceeds one in magnitude is important as this may exclude a number of potential algorithms. A convenient algorithm would also have a uniform space and time step, consistent with those appropriate to typical numerical hydrodynamic models that describe flow in the estuarine channel. A complete water quality model of an estuary couples a mass transport stage to a preceding hydrodynamic stage through the space and time dependent stream flow.

Most published finite element algorithms for initial value problems are finite element in space only and finite difference in time. Higher-order shape functions in space are often associated with the lowest-order finite difference approximation in time, which is broadly equivalent to linear shape functions in time. Outright adoption of space–time finite elements clarifies the order of approximation involved in the solution algorithm and facilitates the introduction of consistent higher-order approximations.

Space–time finite elements for transient field problems were first proposed by Oden[1] and Zienkiewicz and Parekh.[2] Successful applications have subsequently been reported by Bruch and Zyvoloski[3,4] for transient groundwater flow and transient heat conduction, by Grotkop[5] and by Taylor and Davis[6] for long wave propagation, and Gray and Pinder[7] for transient groundwater flow. Only Taylor and Davis considered convective transport but their study was not sufficiently extensive to include any discussion of numerical dispersion and solution oscillation difficulties.

SIMPLIFIED EQUATION FORMULATION

For a constant cross-sectional geometry, mass concentration of a pollutant in solution is described by the simplified estuarine mass transport equation

$$\frac{\partial C}{\partial t}+U\frac{\partial C}{\partial x}=E\frac{\partial^2 C}{\partial x^2}-RC-S \tag{1}$$

where $C(x, t)$ is the slowly-varying concentration of the dispersive substance, t is time, x is the longitudinal co-ordinate along the estuarine channel, R is the linear reaction rate coefficient for the particular substance and S is a source or sink for that substance. Equation (1) is the classical one-dimensional convection–dispersion equation. In subsequent consideration of this equation U, E, R and S are all assumed to be constant.

In the light of the introductory discussion a numerical solution to equation (1) in terms of the uniform rectangular space–time finite elements shown in Figure 1 is sought. An appropriate integral formulation consistent with equation (1) is achieved through the method of weighted residuals.[8] The concentration field $C(x, t)$ within each rectangular element of the complete solution domain Ω is represented by the piecewise continuous approximation in space and time:

$$C(x, t) \doteqdot \hat{C}(x, t) = [N]^T\{c\} \tag{2}$$

where $[N(x, t)]$ is the vector of shape or interpolating or basis functions and $\{c\}$ is the vector of element nodal parameters. The shape functions must be continuous within and between elements and satisfy the essential boundary conditions on equation (1).

Nodal continuity of the field variable $C(x, t)$ is represented by the C^{K_1,K_2} notation, which

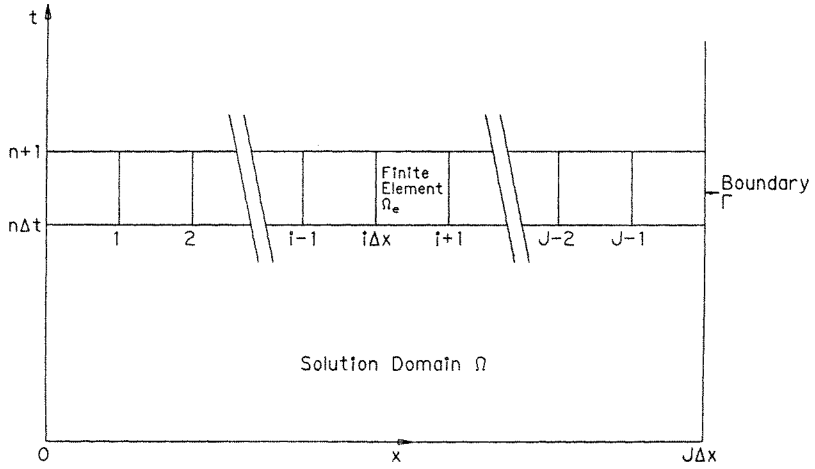

Figure 1. Uniform rectangular space–time finite element in solution domain

implies continuity of all derivatives

$$\frac{\partial^{k_1+k_2}C}{\partial x^{k_1}\,\partial x^{k_2}}$$

at each (i, n) node for $0 \leqslant k_1 \leqslant K_1$, $0 \leqslant k_2 \leqslant K_2$. There are a total of $K = K_1 + K_2 + 1$ nodal parameters at each node, the kth being $k = k_1 + k_2 + 1$. For example $C^{0,0}$ continuity implies continuity of the field variable alone, whereas $C^{1,1}$ implies continuity of the x and t derivatives as well.

$\hat{C}(x, t)$ is an approximate solution to equation (1) so that the residual will in general be non-zero and must be minimized over the solution domain. The method of weighted residuals defines a set of distinct weighting functions $W^{jk}(x, t)$ such that the weighted integral of the residual over the complete solution domain is zero. The number of separate weighting functions is chosen equal to the number of unknown nodal parameters, yielding a closed set of equations in the unknown nodal parameters. In the Galerkin method, the weighting functions are the shape functions $N(x, t)$. Equation (1) becomes

$$\iint_{\Omega} \left[W^{jk}\left(\frac{\partial \hat{C}}{\partial t} + R\hat{C} + S\right) - \frac{\partial W^{jk}}{\partial x}\left(U\hat{C} - E\frac{\partial \hat{C}}{\partial x}\right)\right] \mathrm{d}x\,\mathrm{d}t - \int_{\Gamma} \left[W^{jk}\left(U\hat{C} - E\frac{\partial \hat{C}}{\partial x}\right)\right]_{x=0}^{x=J\Delta x} \mathrm{d}t = 0, \tag{3}$$

where Γ is the boundary of the solution domain. In the normal manner of assigning the weighting functions, the W^{jk} are identically zero at both $x = 0$ and $x = J\,\Delta x$ and the boundary integral term in equation (3) is therefore identically zero.

Integration over the complete solution domain is equivalent to summation of the integration over each separate element, Ω_e, and the solution domain is extended by Δt each time step. An appropriate recurrence relationship to advance the numerical solution in time is established by subtracting the domain integral at time $n\,\Delta t$ from the domain integral at time

$(n+1)\,\Delta t$, giving

$$\sum_{i=0}^{J-1} \iint_{\Omega_e} \left[W^{ik}\left(\left[\frac{\partial N}{\partial t}\right]^T + R[N]^T \right) - \frac{\partial W^{ik}}{\partial x} \left(U[N]^T - E\left[\frac{\partial N}{\partial x}\right]^T \right) \right] \mathrm{d}x\,\mathrm{d}t * \{c\} = -\sum_{i=0}^{J-1} \iint_{\Omega_e} W^{ik} S\,\mathrm{d}x\,\mathrm{d}t \tag{4}$$

where it is implicit that the solution domain has been restricted to the strip of width Δt between $n\,\Delta t$ and $(n+1)\,\Delta t$ sketched in Figure 1. This has the form of a matrix equation $AX = B$. If there are K unknown parameters at each (i, n) node, then the solution vector X and the constants vector B have dimensions 1 by $(J-1)K$ and the coefficient matrix A is square (and banded) with dimensions $(J-1)K$ by $(J-1)K$. The solution vector contains the $(J-1)K$ unknown nodal parameters at the new time $(n+1)\,\Delta t$.

GENERAL EQUATION FORMULATION

The complete equation describing mass transport in a one-dimensional estuarine channel is

$$\frac{\partial}{\partial t}(AC) + \frac{\partial}{\partial x}(QC) = \frac{\partial}{\partial x}\left(AE\frac{\partial C}{\partial x}\right) - RAC - AS \tag{5}$$

Both cross-sectional area A and channel discharge Q, as well as the mass concentration C, vary in space and time, but nodal values of A and Q are available from the numerical hydrodynamic model stage. Within each rectangular element of the complete solution domain, C, A and Q are represented by consistent piecewise continuous approximations in space and time:

$$C(x, t) \div \hat{C}(x, t) = [N]^T\{c\} \tag{6a}$$

$$A(x, t) \div \hat{A}(x, t) = [N]^T\{a\} \tag{6b}$$

$$Q(x, t) \div \hat{Q}(x, t) = [N]^T\{q\} \tag{6c}$$

where $\{c\}$, $\{a\}$, $\{q\}$ are vectors of element nodal parameters for concentration, area and discharge respectively.

The weighted residuals formulation follows along the lines outlined above, leading to the recurrence relationship

$$\begin{aligned}
&\left(\{a\}^T * \sum_{i=0}^{J-1} \iint_{\Omega_e} \left(W^{ik}[N]\left[\frac{\partial N}{\partial t}\right]^T + W^{ik}\left[\frac{\partial N}{\partial t}\right][N]^T + W^{ik}R[N][N]^T - \frac{\partial W^{ik}}{\partial x} E[N]\left[\frac{\partial N}{\partial x}\right]^T \right) \mathrm{d}x\,\mathrm{d}t \right. \\
&\qquad \left. - \{q\}^T * \sum_{i=0}^{J-1} \iint_{\Omega_e} \frac{\partial W^{ik}}{\partial x}[N][N]^T\,\mathrm{d}x\,\mathrm{d}t \right) * \{c\} = -\{a\}^T * \sum_{i=0}^{J-1} \iint_{\Omega_e} W^{ik}[N]S\,\mathrm{d}x\,\mathrm{d}t
\end{aligned} \tag{7}$$

This has the same matrix form as the simplified equation, except that the coefficient matrix A is no longer constant but depends on the $\{a\}$ and $\{q\}$ vectors supplied by a hydrodynamic model. The separate summations of element integrals in equation (7) are invariant, however, for constant R and E.

Formulation of the numerical solution is completed or closed by the specification of appropriate initial and boundary conditions on the dependent variable $C(x, t)$. The initial conditions describe the solution line at time zero and are represented through the nodal parameters $\{c\}_i^0$ for $i=0,1,2,\ldots,J-1,J$. These must be specified or assumed to initiate a simulation. The boundary conditions describe the time history of the environment from which the solution domain is extracted, or more specifically the solution lines at both ends of the particular estuarine reach for all simulation time. These are represented through the nodal parameters $\{c\}_0^n$ and $\{c\}_J^n$ for $n=1,2,\ldots,$ which must be specified at each new time level. A detailed discussion of boundary conditions is given by Sobey and Vidler[9] in the context of the method of characteristics.

DOUBLE ELEMENT ASSEMBLAGE

The assemblage of matrix equations (4) or (7) requires completion of the element double integrations and associated summations. Anticipating that the weight functions as well as the shape functions are unity at the relevant node and vary in some manner to zero at immediately adjacent nodes, beyond which they remain zero, it is clear that non-zero entries for each distinct weighting function W^{jk} are restricted to the six nodes of the double element centred at $j\,\Delta x$, as shown in Figure 2. If there are K nodal parameters $\left(\text{e.g. } C, \frac{\partial C}{\partial x}, \frac{\partial C}{\partial t}, \ldots\right)$ at each node, the subscript k denotes the kth of these.

It is convenient to adopt a double element node numbering system, from 1 to 6 for each double element as shown also in Figure 2. For each double element (or each $j=1,2,\ldots,J-1$) and each nodal parameter (or each $k=1,2,\ldots,K$), equations (4) and (7) yield a linear algebraic equation in all the nodal parameters of the double element, of the form

$$A^{jk}_{2l}c^{j}_{2l}+A^{jk}_{4l}c^{j}_{4l}+A^{jk}_{6l}c^{j}_{6l}=B^{jk} \tag{8}$$

where $B^{jk}=-A^{jk}_{1l}c^{j}_{1l}-A^{jk}_{3l}c^{j}_{3l}-A^{jk}_{5l}c^{j}_{5l}$. Tensor summation notation is assumed with $l=1,2,\ldots,K$. Equation (8) is the general representation of a single row of the matrix equations (4) and (7). The source/sink term has been excluded from the right-hand side of equation (8) and it will not be further considered here.

The resulting coefficient matrix is generally asymmetric but banded. For conservative pollutants it has a constant bandwidth of $3K$ and for $K=1$ the matrix equation might be solved by the Thomas or tri-diagonal algorithm. A variable bandwidth solution algorithm, however, is more appropriate for the complete problem. A suitable subprogram is UACTCL (written by R. L. Taylor and described in Reference 8) or LEQT1B from the IMSL package.

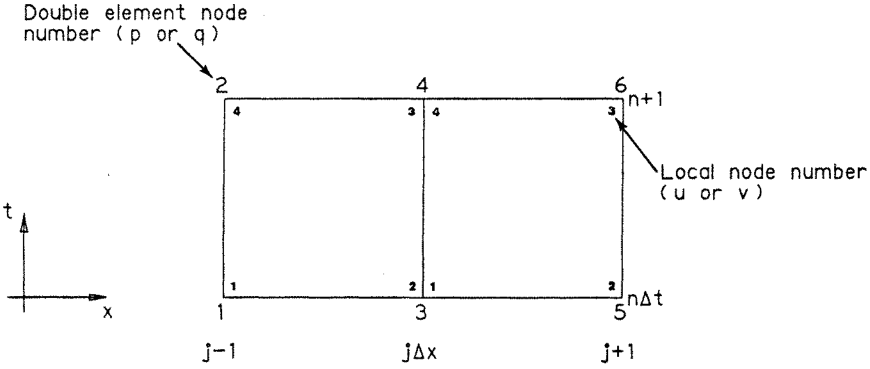

Figure 2. Double element at $j\,\Delta x$

The coefficients A_{pl}^{jk} in equation (8) are determined directly from the element double integrations and subsequent summations. The integrations are completed one component at a time. Each element double integral is first transformed from the global x, t co-ordinate system to the local or natural r, s co-ordinate system and integrations are then completed numerically. Each separate integral in equation (4) has the general form

$$\iint_{\Omega_e} \left[W_{uk}(x,t)\left\{\frac{\partial N_{vl}}{\partial t}(x,t)+RN_{vl}(x,t)\right\}-\frac{\partial W_{uk}}{\partial x}(x,t)\left\{UN_{vl}(x,t)-E\frac{\partial N_{vl}}{\partial x}(x,t)\right\}\right] \mathrm{d}x\,\mathrm{d}t$$

where

$$u, v = \text{local node number} = 1, 2, 3, 4$$

and

$$k, l = \text{number of nodal parameter} = 1, 2, \ldots, K.$$

K, for example, is one when the nodal parameters are restricted to concentration alone. Transforming to the local co-ordinate system and multiplying through by the constant $2/\Delta x$ defines the dimensionless element integral

$$I_{uk,vl} = \int_{-1}^{+1}\int_{-1}^{+1}\left[W_{uk}(r,s)\left\{\frac{\partial N_{vl}}{\partial x}(r,s)+ +\tfrac{1}{2}R\,\Delta t N_{vl}(r,s)\right\}\right.$$
$$\left. -\frac{\partial W_{uk}}{\partial r}(r,s)\left\{\frac{U\,\Delta t}{\Delta x}N_{vl}(r,s)-2\frac{E\,\Delta t}{\Delta x^2}\frac{\partial N_{vl}}{\partial r}(r,s)\right\}\right]\mathrm{d}r\,\mathrm{d}s \quad (9)$$

Each such definite integral is evaluated numerically by Gaussian quadrature.[8] Shape and weighting functions are mostly polynomials and the order of Gauss quadrature can be chosen to achieve exact integration in such cases.

The coefficients A_{pl}^{jk} are finally established by completing the appropriate element summations in equation (4). These summations have been summarized in the form of a double element assemblage table, Table I, in which the coefficients are determined by summing the separate columns. For example,

$$A_{3l}^{jk} = I_{2k,2l} + I_{3k,2l} + I_{1k,1l} + I_{4k,1l} \quad (10)$$

Only the subscripts of I have been listed in the table. Determination of the coefficients A_{pl}^{jk} for the general equation (7) follows the same pattern as above. The discharge Q and the

Table I. Double element assemblage for simplified equation

Local nodes—						
R.H. element			$1l$	$4l$	$2l$	$3l$
L.H. element	$1l$	$4l$	$2l$	$3l$		
Double element nodes, p	$1l$	$2l$	$3l$	$4l$	$5l$	$6l$
Weighting function						
$2k$	$2k, 1l$	$2k, 4l$	$2k, 2l$	$2k, 3l$		
$3k$	$3k, 1l$	$3k, 4l$	$3k, 2l$	$3k, 3l$		
$1k$			$1k, 1l$	$1k, 4l$	$1k, 2l$	$1k, 3l$
$4k$			$4k, 1l$	$4k, 4l$	$4k, 2l$	$4k, 3l$
Coefficients, A_{pl}^{jk}	A_{1l}^{k}	A_{2l}^{k}	A_{3l}^{k}	A_{4l}^{k}	A_{5l}^{k}	A_{6l}^{k}

cross-sectional area A vary with position and time, in a manner described by nodal vectors $\{q\}$ and $\{a\}$ respectively. Two, rather than one, separate element integrations need to be completed. Details can be found in Sobey and Vidler.[9]

HIGHER-ORDER SHAPE FUNCTIONS

Subsequent consideration of space–time finite elements will be restricted to the simplified equation (1) or more precisely the associated weighted residuals statement, equation (4). The essential character of the physical problem and the associated numerical difficulties are both retained and the simplified equation is an appropriate framework for further evaluation.

Linear shape functions (see Figure 3(a)) with $C^{0,0}$ nodal continuity and Galerkin weighting functions lead to discrete equations that are identical with those derived by the finite difference method using lowest-order centred finite difference approximations.[10] The result would be questioned of course if this were not the case, as it is the same physical problem to the same order of approximation. It is immediately apparent, from the finite difference experience, that the finite element formulation of itself will not alleviate the numerical dispersion difficulties. Additional information, specifically a more complete local description of the continuous field variable, implies the local partial derivatives to an appropriate order, namely $\frac{\partial C}{\partial x}, \frac{\partial C}{\partial t}$ and $\frac{\partial^2 C}{\partial x^2}, \frac{\partial^2 C}{\partial x\, \partial t}, \frac{\partial^2 C}{\partial t^2}$ etc., as well as the local field value of C.

It is axiomatic that higher-order numerical algorithms will involve higher-order derivatives than those in the partial differential equation. If linear elements are retained, discrete approximations to these higher derivatives must be based on rather distant grid or nodal points, nodal points that may well be beyond the domain of physical influence and too distant to have any physical influence on the local field variable. This is not the kind of additional information sought and it follows that nodal values of concentration alone (i.e. $C^{0,0}$ nodal continuity in FEM terminology) are an insufficient description of the local field

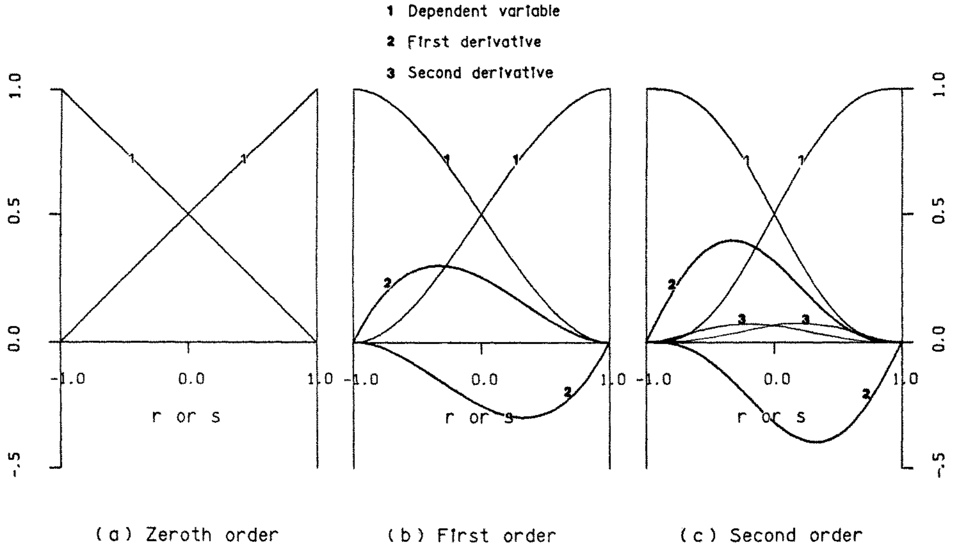

(a) Zeroth order (b) First order (c) Second order

Figure 3. Hermitian shape functions

variable. The additional information sought must be local, within and not beyond the domain of physical influence. It is required within each element. Higher-order space–time finite elements fulfil this prescription almost exactly. In the present context the finite element method has the additional merit of providing a convenient framework for numerical experiment. It is precisely the above motivation that led Fischer[11] and Holly and Preissman[12] to introduce higher-order interpolation in an explicit method of characteristics algorithm. Their results are very encouraging.

Within the framework of rectangular space–time finite elements, higher-order approximations develop naturally along three different lines. The 'serendipity' and Lagrange families maintain $C^{0,0}$ nodal continuity and establish higher-order representation by systematically increasing the number of boundary nodes (serendipity family) and boundary and internal nodes (Lagrange family). The quadratic and cubic serendipity elements are quite common in the FEM literature. For the Hermitian family, higher-order approximations develop from higher-order nodal continuity C^{K_1,K_2} associated with piecewise Hermite interpolation for the partitioned interval. In all three families, the lowest-order member is the linear element in Figure 3(a).

The present study concentrates attention on the Hermitian family, a choice based intuitively on the explicit higher-order continuity at the corner nodes of the basic rectangular element. Equivalent serendipity or Lagrange elements may perform equally well (or bad) but this was not considered. The finite element experience is based predominantly on equilibrium or boundary value problems in structural engineering, where quadratic and cubic serendipity elements have found considerable acceptance. Hermitian shape functions have been used successfully by Bogner *et al.*[13] for plate bending and Cavendish *et al.*[14] for steady-state petroleum reservoir flow, but have found little general acceptance for such problems. Estuarine mass transport is a propagation or initial value problem and the structural engineering experience is of course not necessarily applicable. It is appropriate, however, to observe that the computational effort is related directly to the number of unknown nodal parameters and those nodal parameters at time $n\,\Delta t$ are not unknown. The degrees of freedom of the element on the other hand is a measure of the order of approximation of the solution over the element. Considering the second member of each family, the quadratic serendipity element has five unknown nodal parameters in eight degrees of freedom and the quadratic Lagrange element has one additional unknown at six and one additional degree of freedom at nine. The Lagrange element thus combines a slightly higher order of approximation with an equivalent increase in computational effort, in accord with an intuitive appreciation of both elements. By comparison, the first-order Hermitian element has significantly higher degrees of freedom at twelve for much the same computational effort as the Lagrange element, both having six unknown nodal parameters. Again this matches the intuitive appreciation of the Hermitian element that led to its preference in the present study.

Hermitian and hybrid-Hermitian elements

The Hermite interpolation polynomials to first and second order are sketched in Figures 3(b) and 3(c) respectively. The resulting shape functions for each nodal parameter over a single rectangular element in the local co-ordinate system are listed in Sobey and Vidler.[9] Consistent dimensions can be maintained among the nodal parameters by non-dimensionalizing the derivatives in terms of $\Delta x/2$ as the length scale and $\Delta t/2$ as the time scale.

The Kth order Hermite interpolation polynomials $H^K_{vl}(q)$ are the $(2K+1)$th-order polynomials in the partitioned interval $q=-1$ to $q=+1$ in which

$$D^k H^K_{1l}(q) = \begin{cases} 1 \text{ for } k=l,\, l=0,1,\ldots,K \text{ and for } q=-1 \\ 0 \text{ for } k \neq l \text{ and for } q=+1 \end{cases} \tag{11a}$$

and

$$D^k H^K_{2l}(q) = \begin{cases} 1 \text{ for } k=l,\, l=0,1,\ldots,K \text{ and for } q=+1 \\ 0 \text{ for } k \neq l \text{ and for } q=-1 \end{cases} \tag{11b}$$

where $D^k = \mathrm{d}^k/\mathrm{d}q^k$. Shape functions defined accordingly enforce nodal continuity to the Kth derivative in the field variable and the additional independent nodal parameters. The magnitude of the functions as sketched in Figure 3(b) gives in addition a rough measure of the magnitude of the higher-order correction to the local value of the field variable by the inclusion of slope as an independent nodal parameter. The sketches in Figure 3(c) tell the same story, indicating the further and smaller correction by the inclusion of the rate of change of slope as an additional nodal parameter. These sketches anticipate a significant reduction in numerical solution error on the introduction of the first-order Hermitian polynomials and a diminishing return from second and higher-order Hermitian polynomials.

A total of four higher-order elements (Elements 2 to 5 of Table II) were defined for further analysis, but only one of these, Element 5, is a complete Hermitian space–time element, the other four being hybrid-Hermitian. The choice of an appropriate element must be based on a compromise between precision and computational effort, the introduction of higher-order elements rapidly increasing the computational effort. For example, the number of unknown nodal parameters increases from one to three to six for zeroth (or linear), first and second-order complete Hermitian elements. The computational effort increases roughly as the cube, from one to 27 to 216 times over, and it is desirable to minimize this computational effort, where this is consistent with adequate precision. The hybrid-Hermitian Elements 2 and 4 were chosen with these computational consequences in mind.

Table II lists five space–time finite elements that have been subjected to detailed evaluation. In all five cases the weighting functions are the shape functions in the Galerkin manner. All five space–time finite elements have been subjected to extensive evaluation and numerical testing over parameter ranges for both the flow parameter $U\,\Delta t/\Delta x$ and the dispersion parameter $E\,\Delta t/\Delta x^2$ that are appropriate for estuarine flows.

Table II. Space–time finite elements investigated

Element number	Nodal continuity	Nodal parameters	Shape functions	
			x	t
1	$C^{0,0}$	C	Linear	Linear
2	$C^{1,0}$	$C, \dfrac{\partial C}{\partial x}\dfrac{\Delta x}{2}$	First-order Hermitian	Linear
3	$C^{2,0}$	$C, \dfrac{\partial C}{\partial x}\dfrac{\Delta x}{2}, \dfrac{\partial^2 C}{\partial x^2}\dfrac{\Delta x^2}{4}$	Second-order Hermitian	Linear
4	$C^{0,1}$	$C, \dfrac{\partial C}{\partial t}\dfrac{\Delta t}{2}$	Linear	First-order Hermitian
5	$C^{1,1}$	$C, \dfrac{\partial C}{\partial x}\dfrac{\Delta x}{2}, \dfrac{\partial C}{\partial t}\dfrac{\Delta t}{2}$	First-order Hermitian	First-order Hermitian

WAVE DEFORMATION ANALYSES

The wave deformation analysis of Leendertse[15] provides an objective evaluation of linear numerical solution algorithms for propagation or initial value problems. In a framework of Fourier Series representations for the physical and the numerical solutions, a measure of the precision of the numerical solution over the complete spectrum of spatial wave numbers is established. The physical solution is the solution to the partial differential equation (1). This solution may be represented as the real part of the Fourier series expansion

$$C(x, t) = \sum_m C_m^* e^{i(\beta_m t + \sigma_m x)} \tag{12}$$

where $\beta_m (= 2\pi/T_m$, T_m being the wave period) is the angular wave frequency and $\sigma_m (= 2\pi/L_m$, L_m being the wave length) the spatial wave number of the mth Fourier component. Equation (1) is linear so that only one component of equation (12) need be considered at a time. Substitution of a single Fourier component, $C^* \exp[i(\beta t + \sigma x)]$, into equation (1) establishes the dispersion relationship for the physical wave

$$\beta = -\sigma U + i[\sigma^2 E + R] \tag{13a}$$

or

$$\beta \, \Delta t = (\sigma \, \Delta x) \frac{U \, \Delta t}{\Delta x} + i\left[(\sigma \, \Delta x)^2 \frac{E \, \Delta t}{\Delta x^2} + R \, \Delta t\right] \tag{13b}$$

Partial derivatives of the physical solution are established by direct differentiation of equation (12), whence

$$\frac{\partial C}{\partial x} = \sum_m i\sigma_m C_m^* e^{i(\beta_m t + \sigma_m x)} \tag{14a}$$

$$\frac{\partial C}{\partial t} = \sum_m i\beta_m C_m^* e^{i(\beta_m t + \sigma_m x)} \tag{14b}$$

and

$$\frac{\partial^2 C}{\partial x^2} = \sum_m -\sigma_m^2 C_m^* e^{i(\beta_m t + \sigma_m x)} \tag{14c}$$

The numerical solution is the solution to the discrete finite element equation (8)

$$A_{1l}^k c_{1l} + A_{2l}^k c_{2l} + A_{3l}^k c_{3l} + A_{4l}^k c_{4l} + A_{5l}^k c_{5l} + A_{6l}^k c_{6l} = 0 \tag{15}$$

where tensor summation notation with $l = 1, 2, \ldots, K$ is assumed. There are K such simultaneous linear algebraic equations, $k = 1, 2, \ldots, K$. While the spirit of the following analyses remains unaltered, the details depend on the number and nature of the nodal parameters. The specific details for Elements 1 and 5 are given below, the remaining elements following exactly the same pattern. The coefficients A_{pl}^k are available from the double element assemblage described above.

Element 1 has $C^{0,0}$ nodal continuity, K is one and c_{pl} is C_p, the nodal concentration. Equation (15) becomes

$$A_1 C_1 + A_2 C_2 + A_3 C_3 + A_4 C_4 + A_5 C_5 + A_6 C_6 = 0 \tag{16}$$

The numerical solution also is represented as the real part of a Fourier Series expansion

$$C_j^n = \sum_m C_m^* e^{i(\beta'_m t + \sigma_m x)} \tag{17}$$

along the lines of equation (12) but allowing the angular wave frequencies β'_m to differ from β_m for the physical solution. Equation (16) is also linear so that only one component of equation (17) need be considered at a time. Substitution of a single Fourier component, $C^* \exp[\mathrm{i}(\beta' t+\sigma x)]$, into equation (16) results in

$$\mathrm{e}^{\mathrm{i}\beta'\Delta t}=\frac{A_1\mathrm{e}^{-\mathrm{i}\sigma\Delta x}+A_3+A_5\mathrm{e}^{\mathrm{i}\sigma\Delta x}}{A_2\mathrm{e}^{-\mathrm{i}\sigma\Delta x}+A_5+A_6\mathrm{e}^{\mathrm{i}\sigma\Delta x}} \tag{18}$$

This is the equivalent dispersion relationship for the numerical or computed wave for Element 1.

Element 5, on the other hand, has $C^{1,1}$ nodal continuity, K is three and the nodal parameters are

$$c_{\mathrm{p}1}=C_{\mathrm{p}} \tag{19a}$$

$$c_{\mathrm{p}2}=\frac{\partial C_{\mathrm{p}}}{\partial x}\frac{\Delta x}{2} \tag{19b}$$

and

$$c_{\mathrm{p}3}=\frac{\partial C_{\mathrm{p}}}{\partial t}\frac{\Delta t}{2} \tag{19c}$$

Each of these parameters is independent and is independently propagated by the solution algorithm. Each is represented by separate Fourier Series expansions. The discrete finite element equation (15) remains linear so that only a single wave number need be considered at a time. The separate Fourier components are:

$$C_{\mathrm{p}}=C^*\mathrm{e}^{\mathrm{i}(\beta'_1 t+\sigma x)} \tag{20a}$$

$$\frac{\partial C_{\mathrm{p}}}{\partial x}\frac{\Delta x}{2}=\mathrm{i}\sigma\frac{\Delta x}{2}C^*\mathrm{e}^{\mathrm{i}(\beta'_2 t+\sigma x)} \tag{20b}$$

$$\frac{\partial C_{\mathrm{p}}}{\partial t}\frac{\Delta t}{2}=\mathrm{i}\beta\frac{\Delta t}{2}C^*\mathrm{e}^{\mathrm{i}(\beta'_3 t+\sigma x)} \tag{20c}$$

The independence of these nodal parameters is represented through separate angular wave frequencies β'_1, β'_2 and β'_3 respectively.

Substituting equations (20) into equation (15) gives

$$D^k\mathrm{e}^{\mathrm{i}\beta'_1\Delta t}+E^k\mathrm{e}^{\mathrm{i}\beta'_2\Delta t}+F^k\mathrm{e}^{\mathrm{i}\beta'_3\Delta t}=G^k \quad \text{for} \quad k=1,2,3 \tag{21}$$

where D^k, E^k, F^k and G^k are complex and functions of $\beta\,\Delta t$, $\sigma\,\Delta x$ and the coefficients A^{jk}_{pl}. They are listed in Sobey and Vidler.[9] Equations (21) represent three simultaneous equations in the complex exponentials $\exp(\mathrm{i}\beta'_1\,\Delta t)$, $\exp(\mathrm{i}\beta'_2\,\Delta t)$ and $\exp(\mathrm{i}\beta'_3\,\Delta t)$ and in which all the constants are also complex. By treating the exponentials as the unknowns and separating them and the constants D^k, E^k, F^k and G^k into real and imaginary parts, equations (21) were reduced to a set of six linear algebraic equations with real coefficients in the real and imaginary parts of the exponentials. This set of equations was solved by matrix inversion.

A complex propagation factor, following Leendertse, is defined as the ratio T of the computed solution to the physical solution after the solution has propagated a certain distance and time. Leendertse's choice of time was $2\pi/\beta$ for long wave propagation but β is complex (see equation (13)) for the convection–dispersion equation and time must be real. The present problem is convection dominated and an appropriate choice of time scale is

$2\pi/\text{Real}\,(\beta)$:

$$T=\frac{e^{i(\beta_1't+\sigma x)}}{e^{i(\beta t+\sigma x)}}=e^{i(\beta_1'-\beta)t}\quad\text{for}\quad t=\frac{2\pi}{-\sigma U}\tag{22}$$

Similar propagation factors can be defined for higher-order modes where they exist but major interest centres on the primary mode. Where T equals one, the solutions of the finite element equation and the partial differential equation correspond. The proximity of T to unity is an established and convenient measure of the precision of a numerical algorithm.

The propagation factor thus defined depends on four dimensionless parameters, the flow parameter $U\,\Delta t/\Delta x$, the dispersion parameter $E\,\Delta t/\Delta x^2$, the decay parameter $R\,\Delta t$ and the dimensionless wave number $\sigma\,\Delta x=2\pi/(L/\Delta x)$. For a particular problem, the flow, dispersion and decay parameters are constant and the complete spectrum of behaviour is established by varying the dimensionless wave number $\sigma\,\Delta x$, or more commonly the dimensionless wave length $L/\Delta x$, over the full range. The dimensionless wave number or wave length is a measure of the steepness of the concentration gradient. A small value of $L/\Delta x$ implies a

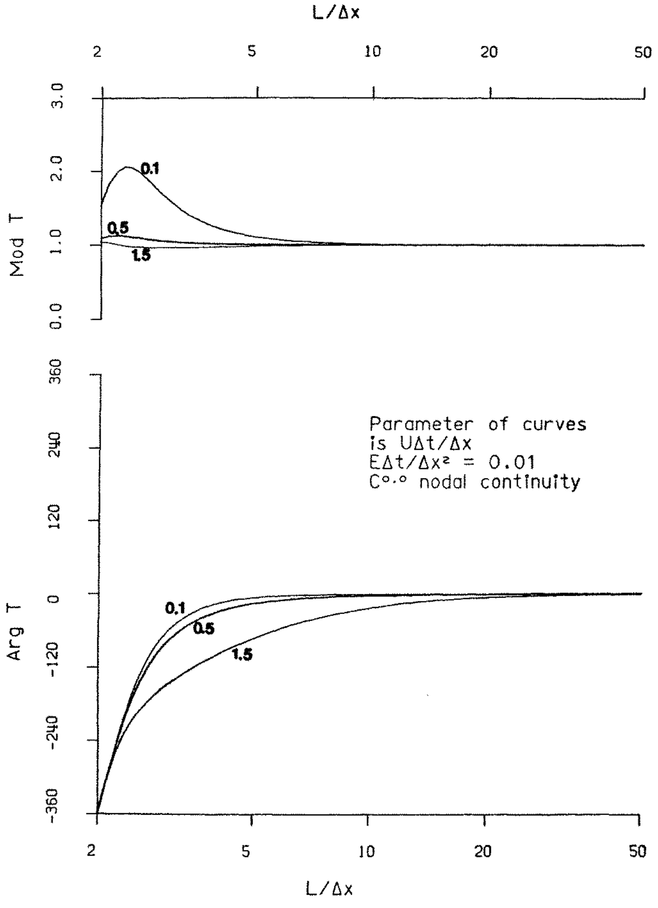

Figure 4. Wave deformation for Element 1

steep gradient and this is where problems are anticipated. The flow and dispersion parameters were grouped in a systematic manner to establish the complete behaviour pattern. Equivalent Peclet Numbers ($U\,\Delta x/E$) range from 0·5 ($U\,\Delta t/\Delta x = 0{\cdot}05$, $E\,\Delta t/\Delta x^2 = 0{\cdot}1$) to 1500 ($U\,\Delta t/\Delta x = 1{\cdot}5$, $E\,\Delta t/\Delta x^2 = 0{\cdot}001$) but it is more appropriate to accord separate significance to the flow and dispersion parameters as they relate to separate terms of equation (1).

A selection of the wave deformation results are presented as Figures 4 to 8 for Elements 1 to 5 respectively. The dispersion parameter is constant at 0·01 for these figures and the parameter identifying each set of curves is the flow parameter. More complete details can be found in Sobey and Vidler.[9] Both the modulus, $|T|$, and the phase, $\arg T$, are plotted separately as functions of $L/\Delta x$. In physical terms, $|T|$ in excess of one implies relative amplification of the computed solution at that wave number, whereas decay is implied for $|T|$ less than one. A phase lag ($\arg T$ negative) implies the particular wave number component is propagated by the numerical solution at a slower speed than the physical solution, a phase lead implying a faster speed. Numerical dispersion and solution oscillations stem from inadequate representation of the higher wave number components of a spatial distribution of

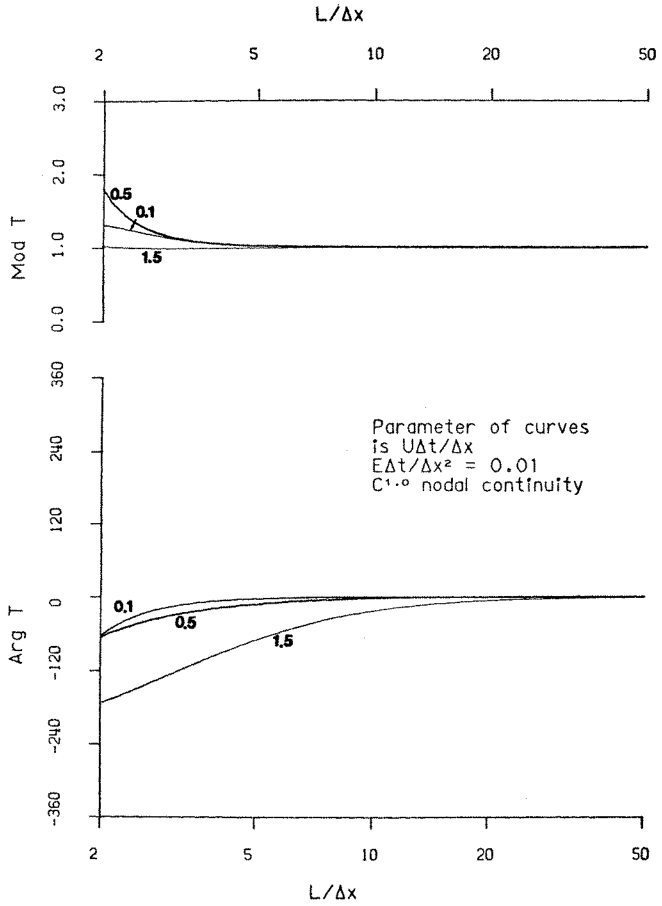

Figure 5. Wave deformation for Element 2

concentration. It follows that major interest centres on the behaviour of the propagation factor for small $L/\Delta x$.

Figure 4 for Element 1, the linear element, gives a ready explanation for its poor performance. There are consistently large amplification and particularly phase errors for the higher wave numbers over the whole range of flow and dispersion parameters. Increasing values of the dispersion parameter progressively reduce the amplitude errors but significant, mostly lagging phase errors remain. Leading phase errors were also observed for small flow parameter and large dispersion parameter (i.e. small Peclet Number).

Element 2 is the first of the hybrid-Hermitian elements, the $C^{1,0}$ nodal continuity being a recognition of the predominance of spatial derivatives in the transient convection–dispersion equation. A sample of the wave deformation characteristics is presented in Figure 5 and is quite encouraging, especially for the lower values of the flow parameter. There is a vast improvement over the Element 1 performance. Amplitude deformation is approaching reasonably tolerable levels over the complete wave number spectrum for all flow parameters considered. There are significant improvements also in the phase characteristics, but only for small flow parameters. There were both lagging and leading phase errors at small $L/\Delta x$ for

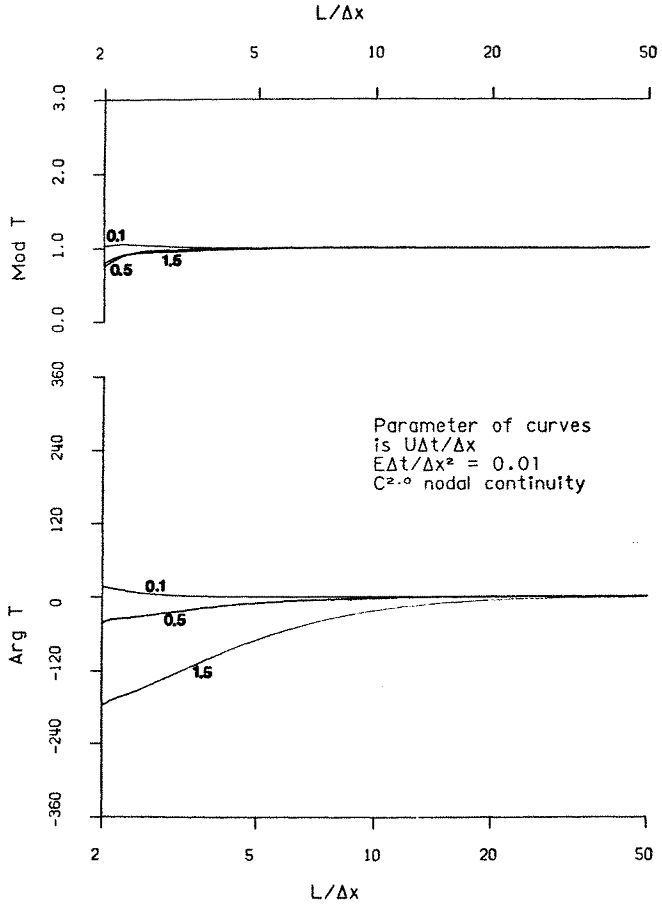

Figure 6. Wave deformation for Element 3

small flow parameters, depending on the dispersion parameter, but lagging errors only for flow parameters of at least 0·5 and above, where the dispersion parameter becomes increasingly unimportant and the phase errors increase in magnitude. The phase errors are unacceptable for flow parameters above about 0·75.

The increasing unacceptability of Element 2 as the flow parameter increases can be related to the characteristic directions. Ignoring dispersion and decay and referring to Figure 9, the solution for C_i^{n+1} is equivalent to interpolation among the nodal parameters to determine the concentration at point p. For smaller flow parameters, p is located between $(i-1, n)$ and (i, n) in the x-direction and separate estimates of nodal values of spatial gradient will lead to higher-order interpolation. As the flow parameter increases beyond one, the point p is located between nodes $(i-1, n)$ and $(i-1, n+1)$ in the t-direction and nodal values of spatial gradient will have little impact on the interpolation for p. The results from Elements 3, 4 and 5 will in turn also be related to Figure 9.

Element 3 has $C^{2,0}$ nodal continuity, having both the first and second spatial gradients as separate nodal parameters. A sample of the wave deformation results is presented as Figure 6. As would be anticipated from Figure 9, there is some improvement in both the modulus

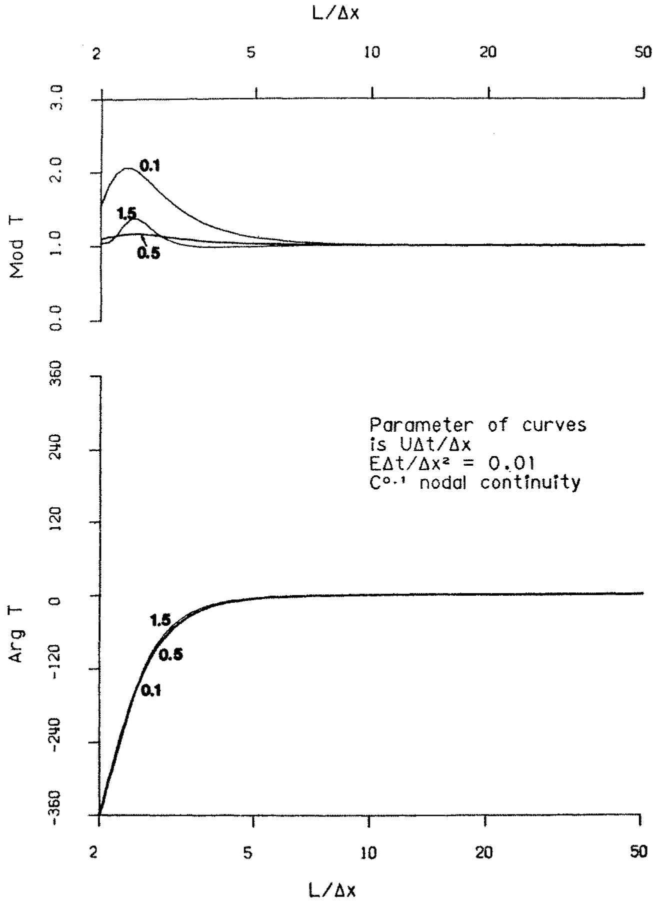

Figure 7. Wave deformation for Element 4

and phase curves for small flow parameters but for large flow parameters the results are almost indistinguishable from those for Element 2. Phase errors for Element 2 at small flow parameters were a combination of leading and lagging errors, depending on the dispersion parameter, but only leading phase errors are predicted for Element 3, regardless of the dispersion parameter. Amplitude errors follow a similar pattern at small flow parameters, a moderate amplification at most for Element 2 and a moderate decay for Element 3.

Element 4 has $C^{0,1}$ nodal continuity, with the time derivative as the second nodal parameter. A sample of the wave deformation results is presented as Figure 7. Compared to Element 2, the results are generally quite disappointing. There is a definite improvement on Element 1 but the element must still be rejected. The errors certainly decrease as the flow parameter increases, as anticipated from the characteristic directions in Figure 9, but the lagging phase errors remain unacceptable. This asymmetry in the x and t behaviour was anticipated, however, from the nature of the terms in the convection–dispersion equation and the knowledge that problems centred on the convective term.

Element 5 has $C^{1,1}$ nodal continuity, including both the time and space derivatives as separate nodal parameters. This is the complete first-order Hermitian space–time element

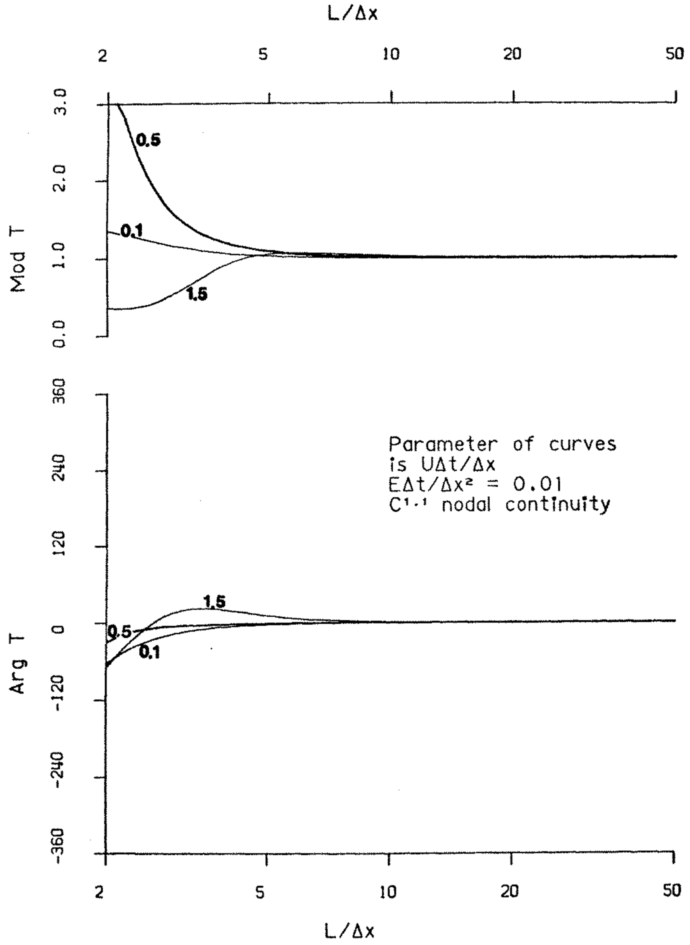

Figure 8. Wave deformation for Element 5

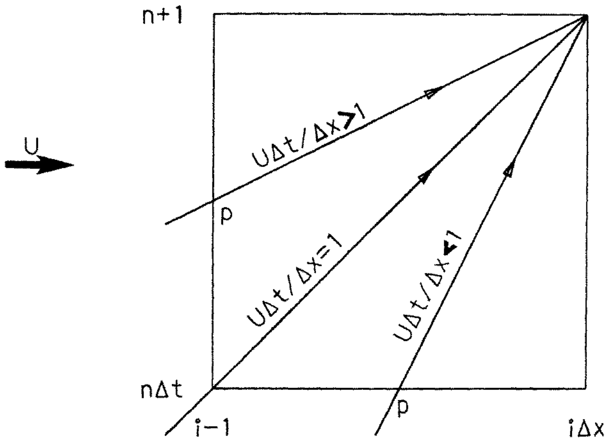

Figure 9. Characteristic directions for different flow parameters

and a sample of the wave deformation characteristics is presented in Figure 8. The phase results are reasonably satisfactory over the complete range of flow parameters, the dispersion parameter having little overall influence. For low flow parameters the behaviour is marginally better than Element 2 ($C^{1,0}$ continuity) and marginally inferior to Element 3 ($C^{2,0}$ continuity). For moderate to large flow parameters, Element 5 is measurably superior. The influence of the flow parameter on the phase errors is quite pronounced, with predominantly lagging phase errors at small flow parameters varying to predominantly leading phase errors for larger flow parameters. The overall behaviour is in accord with the characteristic directions in Figure 9, the higher order respresentations in space and time being consistent with higher-order interpolation for the point p at flow parameters less than and greater than one.

It would appear from the wave deformation results that a complete Hermitian, rather than a hybrid-Hermitian, space–time element is essential to achieve a reasonable numerical solution to the convection–dispersion equation over the complete range of flow parameters. The question of what order, however, remains. Element 5 is a complete first-order Hermitian element. The next step is a complete second-order Hermitian element. This element has six nodal parameters—C; $\frac{\partial C}{\partial x}, \frac{\partial C}{\partial t}; \frac{\partial^2 C}{\partial x^2}, \frac{\partial^2 C}{\partial x\,\partial t}, \frac{\partial^2 C}{\partial t^2}$—compared to three—$C$; $\frac{\partial C}{\partial x}, \frac{\partial C}{\partial t}$—for Element 5. The number of unknowns are doubled and the computational effort would increase by a factor of eight, almost an order of magnitude. There is of course a measure of diminishing returns from increasingly higher-order approximations. A comparision of Element 1 ($C^{0,0}$ nodal continuity), Element 2 ($C^{1,0}$) and Element 3 ($C^{2,0}$) gives a rough measure of the return that might be expected. The phase error becomes increasingly smaller with each increase in order but the improvement in precision is somewhat less than an order of magnitude for each order.

NUMERICAL EXPERIMENTS

The final evaluation of the selected space–time elements was a set of numerical experiments comparing the performance of the separate elements with an analytical solution to equation (1). Decay and source/sink terms were neglected in these tests and the context is the convection and dispersion of an instantaneous point source of mass M at time zero. The analytical solution is

$$C(x,t)=\frac{M}{\rho A\sqrt{(4\pi Et)}}\exp\left[-\frac{(x-Ut)^2}{4Et}\right] \tag{23}$$

where ρ is the mass density of the water and A the constant cross-section of the channel. Equation (23) describes a Gaussian distribution whose centre of mass convects at speed U, whose peak concentration decays as $(Et)^{-\frac{1}{2}}$ and whose half width increases as $(Et)^{\frac{1}{2}}$.

The initial conditions for the numerical experiments cannot be set at time zero as an instantaneous point source cannot be resolved by a computational grid. The initial conditions have been defined at time t_0 when the half width of the distribution has grown to $S\,\Delta x$, where S is a dimensionless constant and a measure of the steepness of the initial profile. The peak concentration at this time has been set at 1·0. The half width of the distribution is the distance b such that

$$C(Ut\pm b,t)=\tfrac{1}{2}C(Ut,t) \tag{24a}$$

i.e. the distance from the peak concentration to the points where the concentration has fallen to half the peak value. From Equation (23)

$$b^2=\frac{4Et}{\ln 2} \tag{24b}$$

The half width is a more identifiable dispersion length scale than the standard deviation $(4Et)^{\frac{1}{2}}$, which appears naturally in equation (23).

It is unrealistic to expect a numerical algorithm to perform beyond the resolution capabilities of the finite grid and associated shape functions. The problem is analogous to aliasing in frequency spectral analysis, where frequencies above the Nyquist or folding frequency[16]

$$\omega_N=2\pi/2\;\Delta t \tag{25}$$

cannot be resolved from a time series with a uniform time step of Δt. Information at frequencies above this Nyquist frequency is folded back to frequencies below the Nyquist frequency. Aliasing in a spatial series sense is encountered here and wave numbers in excess of the Nyquist wave number

$$\sigma_N=2\pi/2\,\Delta x \tag{26}$$

are folded back to smaller wave numbers less than σ_N. In terms of wave length, the Nyquist wave length would be $L_N=2\,\Delta x$ and wave lengths below L_N cannot be resolved. Equation (26) is strictly applicable to $C^{0,0}$ nodal continuity. Higher-order nodal continuity will extend the spatial resolution to shorter wave lengths than $2\,\Delta x$ but a finite Nyquist wave number will nonetheless exist, dependent solely on the space step and the order of nodal continuity.

In the sense that $2b$ is a measure of the wave length, an initial S of order one would provide an appropriate test of the separate elements. An S value of 0·5 was adopted for the following tests. These initial distributions are dominated by the shorter wave lengths and provide quite demanding tests of operational performance. In addition the Gaussian hump distribution will discern both leading and lagging phase errors at the upstream and downstream edges respectively. A common alternative numerical test bed for the convection–dispersion equation is the propagation of a continuous point source, in effect the convection and dispersion of a concentration front. However, this distribution has a leading edge only

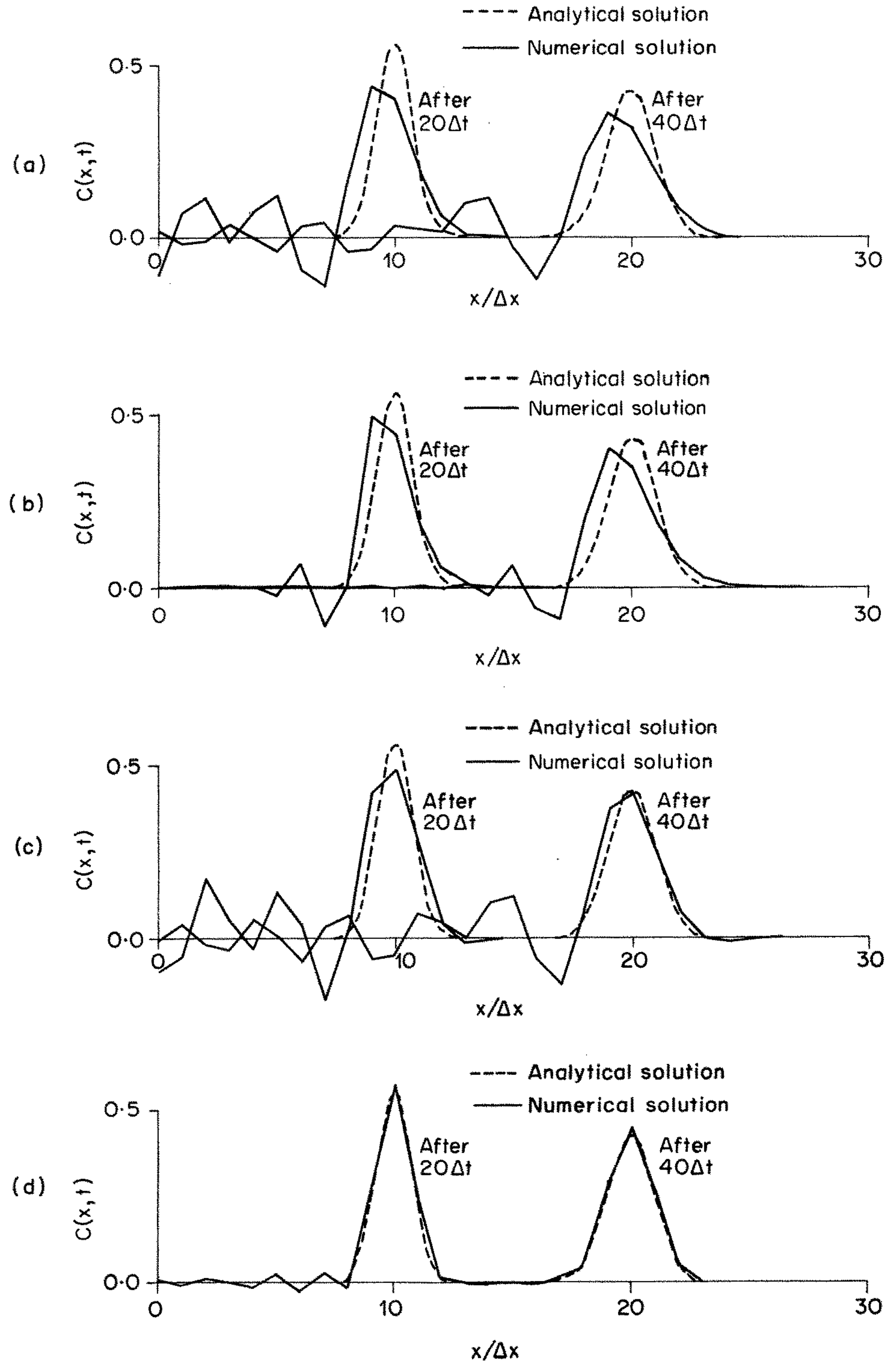

Figure 10. Comparison of numerical experiments: (a) Element 1 ($C^{0,0}$ nodal continuity); (b) Element 2 ($C^{1,0}$ nodal continuity); (c) Element 4 ($C^{0,1}$ nodal continuity); (d) Element 5 ($C^{1,1}$ nodal continuity)

and is not quite as demanding or revealing as the steep Gaussian hump, which has both a leading and trailing edge.

A wide range of numerical experiments is reported in Sobey and Vidler[9] and a representative sample is included here as Figure 10, showing four of the five elements at a flow parameter of 0·5 and a dispersion parameter of 0·01. The analytical and numerical solutions are compared after 20 and 40 time steps respectively. Element 3 has been omitted because of its close performance characteristics to Element 2. The grid resolution of the initial conditions does not allow an exact match with the Gaussian curve, but this is unavoidable and must be borne in mind when evaluating the results. As anticipated, the numerical experiment results are in complete agreement with the wave deformation curves. The numerical experiments do serve, however, to put the wave deformation analyses in reasonable perspective, giving some physical reality to amplitude errors and particularly leading and lagging phase errors.

Element 1 shows a consistent pattern of substantial trailing edge solution oscillations coupled with peak amplitude decay and phase lag, a skewed profile being observed over the complete flow parameter range. The equivalent wave deformation, Figure 4, showed a persistent phase lag that is entirely consistent with the trailing edge oscillations. The numerical dispersion is a consequence of the re-distribution of mass to the trailing edge oscillations. The Element 2 results, Figure 10(b), were quite impressive at very low flow parameters[9] but rapidly degenerated to common skewed profiles with trailing edge oscillations at moderate to high flow parameters. Again these results are as anticipated from the wave deformation analyses where the phase characteristics are favourable only at small flow parameters. In plotting the results for Element 2, no advantage was taken of the available nodal estimates for the spatial gradients and linear interpolation between nodal field values was assumed. If the spatial gradients had been used in the interpolation, the results would appear more satisfactory, particularly around the peak.

The Element 4 response in Figure 10(c) was again as anticipated. The wave deformation characteristics are never really acceptable but become increasingly better at higher flow parameters. Exactly the same trend is observed with the Gaussian hump experiments. Once again the Element 5 response, in Figure 10(d), was as anticipated. The wave deformation analyses are quite reasonable across the complete flow parameter range and this is clearly reflected in the Gaussian hump experiments. As with Element 2, no advantage was taken of the spatial gradients in plotting the numerical results. Solutions oscillations of course remain, as the wave deformation characteristics are not perfect, but the magnitude of the errors is approaching tolerable limits. A complete second-order Hermitian element would further reduce such problems but at the expense of significantly increased computational effort.

CONCLUSIONS

A detailed evaluation of the potential of space–time finite elements in numerical solutions of the convection–dispersion equation has highlighted the difficulties that persist where an Eulerian framework is maintained. As a general comment, the value of wave deformation analyses is clearly identified. Lagging phase errors lead to trailing edge oscillations and an upstream skewing of the concentrating distribution. Leading phase errors have the reverse effect, leading edge oscillations and a downstream skewing of the distribution. Higher-order elements generally lead to reasonably satisfactory amplitude performance and the phase errors have been identified as the critical aspect of wave deformation in this context. More specifically the numerical solution difficulties have been clearly related to the wave deformation characteristics at the lowest wave lengths. It is unrealistic, however, to expect a performance that is beyond the resolution capabilities of the grid. Wave numbers above the Nyquist wave number cannot be resolved at $C^{0,0}$ nodal continuity. HIgher-order nodal continuity enhances spatial resolution but the concept of a Nyquist wave number remains.

The separate dependence of any numerical solution algorithm on three dimensionless groups, respectively the flow, dispersion and decay parameters, is also identified. The flow parameter dominates the numerical solution performance. The dispersion parameter has a quite secondary importance, while it remains small, and the decay parameter has no noticeable effects in the range considered. From the five elements considered, it would seem that the complete first-order Hermitian space–time element is a reasonable compromise between adequate precision and acceptable computational effort, but only where there is appropriate resolution of the shorter wave lengths.

REFERENCES

1. J. T. Oden, 'A general theory of finite elements II. Applications', *Int. j. numer. methods eng.*, **1,** 247–259 (1969).
2. O. C. Zienkiewicz and C. J. Parekh, 'Transient field problems: two dimensional and three dimensional analysis by isoparametric finite elements', *Int. j. numer. methods eng.*, **2,** 61–71 (1970).
3. J. C. Bruch and G. Zyvoloski, 'Finite element solutions of unsteady and unsaturated flow in porous media', in *Mathematics of Finite Elements and Applications* (Ed. J. R. Whiteman), Academic Press, New York, 1971, pp. 201–211.
4. J. C. Bruch and G. Zyvoloski, 'Transient two-dimensional heat conduction problems solved by the finite element method', *Int. j. numer. methods eng.*, **8,** 481–494 (1974).
5. G. Grotkop, 'Finite element analysis of long-period water waves', *Comput. Methods Appl. Mech. and Eng.*, **2,** 147–157 (1973).
6. C. Taylor and J. Davis, 'Tidal and long wave propagation—a finite element approach', *Comput. and Fluids*, **3,** 125–148 (1975).
7. W. G. Gray and G. F. Pinder, 'Galerkin approximation of the time derivative in the finite element analysis of groundwater flows', *Wat. Resour. Res.*, **10,** 821–828 (1974).
8. O. C. Zienkiewicz, *The Finite Element Methods*, 3rd edn, McGraw-Hill, London, 1977.
9. R. J. Sobey and.P. F. Vidler, 'Numerical modelling of mass transport in well-mixed estuaries', *Dept. Civil and Systems Eng., James Cook Univ., Res. Bull. CS19* (1980).
10. H. L. Stone and P. L. T. Brian, 'Numerical solution of convective transport problems', *A.I.Ch.E.Jl.*, **9,** 681–688 (1963).
11. K. Fischer, 'Convective difference schemes and Hermite interpolation', *Int. j. numer. methods eng.*, **12,** 930–940 (1978).
12. F. M. Holly and A. Preissman, 'Accurate calculation of transport in two dimensions', *J. Hydraul. Div., ASCE,* **103,** 1259–1278 (1977).
13. F. K. Bogner, R. L. Fox and L. A. Schmit, 'The generation of interelement-compatible stiffness and mass matrices by the use of interpolation formulas', *Proc. Conf. Matrix Methods in Structural Mechanics*, Dayton, Ohio, 397–443 (1965).
14. J. C. Cavendish, J. S. Price and R. S. Varga, 'Galerkin methods for numerical solution of boundary value problems', *J. Soc. Petrol. Eng.* (*AIME*), **9,** 204–220 (1969).
15. J. J. Leendertse, 'Aspects of a computational model for long-period water-wave propagation', Rand Corp., Santa Monica, *RM-5294-PR*, May (1967).
16. A. S. Bendat and A. G. Piersol, *Random Data: Analysis and Measurement Procedures*, Wiley-Interscience, New York, 1971.